The impacts of a weakened Atlantic Meridional Overturning Circulation on ENSO in a warmer climate

Wei Liu[1*], David Duarte Cavalcante Pinto[1], Alexey Fedorov[2,3], Jiang Zhu[4]

[1]Department of Earth and Planetary Sciences, University of California Riverside, Riverside, CA, USA
[2]Department of Earth and Planetary Sciences, Yale University, New Haven, CT, USA
[3]LOCEAN/IPSL, Sorbonne University, Paris, France
[4]Climate and Global Dynamics Laboratory, National Center for Atmospheric Research, Boulder, CO, USA

*Corresponding author: Wei Liu (wei.liu@ucr.edu)

Key Points: (limit to 140 characters)

- A. Relative to the simulated future state with reduced ENSO variability, AMOC slowdown strengthens ENSO by amplifying Ekman upwelling feedback.
- B. AMOC slowdown facilitates the occurrence of Central Pacific El Niño events.
- C. AMOC impacts on ENSO are smaller than model internal variability during the twenty-first century.

Abstract

This study quantifies the impacts of the Atlantic Meridional Overturning Circulation (AMOC) on the El Niño–Southern Oscillation (ENSO) under anthropogenic warming by comparing climate change model simulations with declining and fixed strengths of the overturning. After the 1980s, a weakened AMOC is shown to reduce the strength of the annual cycle of sea surface temperature (SST) in the eastern equatorial Pacific and induce anomalous cross-equatorial northerly winds there, which strengthens ENSO variability by about 11%. An analysis of the Bjerknes stability index reveals that this intensification of ENSO results mainly from enhanced Ekman upwelling feedback due to amplified atmospheric wind response to SST anomalies and oceanic upwelling response to equatorial wind stress anomalies. The weakened AMOC also promotes the occurrence of Central Pacific El Niño events and reduces ENSO skewness. These AMOC impacts on ENSO magnitude and complexity throughout the twenty-first century are however smaller than ENSO variations expected from internal climate variability.

Plain Language Summary

Here, we use climate model simulations to study how changes in the Atlantic Meridional Overturning Circulation (AMOC) influence the El Niño–Southern Oscillation (ENSO) in a warming climate. We find that the overturning circulation slowdown caused by global warming can strengthen the ENSO variability by about 11% over 1981–2100 by reducing the annual cycle of sea surface temperature and cross-equatorial winds in the eastern equatorial Pacific. The detailed physical mechanism explaining this ENSO intensification involves changes in ocean-atmosphere feedback. We also find that the declining AMOC makes El Niño events with the Central Pacific temperature pattern more frequent. The above effects of the AMOC on ENSO are however smaller than differences expected from model internal climate variability.

1. Introduction

The Atlantic Meridional Overturning Circulation (AMOC) plays a crucial role in Earth's climate (Bryden & Imawaki 2001; Liu et al. 2017). This ocean circulation system has been observed to slow down over the past two decades as measured by the RAPID array at 26.5^{o}N in the North Atlantic (Frajka-Williams 2015; Smeed et al. 2018); however, given the relatively short observational period, this AMOC slowdown can be part of natural climate variability (Robert et al. 2014). According to some proxy reconstructions, the AMOC slowdown might have started as early as in the middle-to-late twentieth century (Rahmstorf et al. 2015; Thornalley et al. 2018; Caesar et al. 2018, 2021); this conclusion however has been debated (Kilbourne et al. 2022). During the twenty-first century, the AMOC is projected to continue to decline as summarized by the Fifth Assessment Report of the Intergovernmental Panel on Climate Change (IPCC AR5). For example, under the RCP8.5 (Representative Concentration Pathway 8.5) global warming scenario, the AMOC strength will decrease by 12–54% by 2100. In the recent IPCC AR6, the AMOC also shows a comparable decline by 2100 under a similar climate scenario of the SSP585 (an updated version of RCP8.5 but now based on Shared Socioeconomic Pathways, c.f., Weijer et al. 2020), although the newer models put the starting time of the AMOC decline by about one decade later due to a stronger anthropogenic aerosol forcing used (Menary et al. 2020; Hassan et al. 2021).

The AMOC slowdown has been shown to impact the global and regional climate (Liu et al. 2020; Ren & Liu 2021; Li & Liu 2022). For example, in the absence of anthropogenic global warming, a weakened AMOC can remotely cause a meridionally asymmetric change in the mean state in the eastern equatorial Pacific through atmospheric teleconnections and local coupled air–sea feedback (Dong & Sutton 2002; Zhang & Delworth 2005), featuring a substantial weakening of sea surface temperature (SST) annual cycle there (Timmermann et al. 2007a) and a reduction in mean cross-equatorial winds (Hu & Fedorov 2018). These changes in the mean state lead in turn to an eastward shift of El Niño–Southern Oscillation (ENSO) SST anomalies, a longer and more regular ENSO period (Willianson et al. 2018) and an increase in the magnitude of ENSO variability (Timmermann et al. 2007a; Dong & Sutton 2007). Yet a recent study (Orihuela-Pinto et al. 2022) argued that a collapsed AMOC acts to decrease, instead of increase, the ENSO variability.

Most of the above insights of AMOC impacts however are obtained from classical freshwater hosing experiments causing a slowdown or a full collapse of the AMOC. To the best of our knowledge, the impacts of projected AMOC slowdown have not been explicitly assessed in the context of anthropogenic warming via fully coupled climate model experiments. Also, it is well recognized that climate model projections of ENSO intensity have large uncertainties (Collins et al. 2010; Stevenson 2012; Cai et al. 2015, 2022) because ENSO is controlled by a delicate balance of amplifying and damping feedback, which is modified by climate change simultaneously (Fedorov & Philander 2000, 2001; Collins et al. 2010; Zheng et al. 2016; Hu & Fedorov 2018; Fedorov et al. 2020). So far, efforts to understand ENSO projections have mainly focused on local processes in the tropic Pacific, whilst remote effects such as those from the future AMOC slowdown have received less

attention. Therefore, it remains unclear how and to what extent the projected AMOC slowdown can affect future ENSO variability during the twenty-first century, which is the focus of the current study.

2. Data and Methods

2.1. Observations

We use four monthly-reconstructed SST datasets to assess historical ENSO variability during 1861–1980. These datasets are COBE-SST2 on a one-degree grid (Hirahara et al. 2014), ERSST.v4 (Huang et al. 2015; Liu et al. 2015) and ERSSTv5 (Huang et al. 2017) on a two-degree grid and KAPLAN EXTENDED v2 on a five-degree grid (Kaplan et al. 1998). We compute the mean over these four SST datasets as well as one standard deviation. For each dataset, we calculate the Niño 3.4 ENSO index by averaging the detrended SST anomalies over the Niño 3.4 area (5^{o}N–5^{o}S, 170^{o}W–120^{o}W). The mean of the Niño 3.4 index depicts a significant ENSO period at 2-4 years during 1861–1980 (Figure 1c).

2.2. Climate model simulations

We employ a broadly used climate model, the Community Climate System Model version 4 (CCSM4) with the standard 1-degree atmospheric resolution (Deser et al. 2012), which captures well the 2-4 year periodicity of ENSO, even though with a larger amplitude (Figure 1c), as well as an annual cycle of SST in the eastern equatorial Pacific similar to the observations (Figure S1). We use five ensemble members of CCSM4 historical and RCP8.5 simulations from 1861 to 2100. Consistent with most of IPCC AR5 model results, CCSM4 simulates a relatively steady AMOC in the early and middle twentieth century (Figure 1a), which is likely due to the compensation between the warming effect of rising greenhouse gases and the cooling effect of growing aerosols at that time (Delworth & Dixon 2006). The model AMOC weakens after the 1980s when aerosol emissions began to decline over North America and Europe while greenhouse gas concentrations continued to rise.

Utilizing CCSM4 historical and RCP8.5 simulations, we conduct a parallel sensitivity experiment with corresponding five ensemble members, which is branched from the year 1980 of the historical simulation and driven by the same historical and RCP8.5 forcings except that a small amount of freshwater is gradually removed from the surface in the subpolar North Atlantic and uniformly redistributed over rest of the global ocean (details are provided in Liu et al. 2020). This experimental setup helps maintain a constant AMOC strength throughout the twenty-first century even under anthropogenic warming (Figure 1a). The AMOC strength is defined as the maximum of the annual mean stream function below 500 m in the North Atlantic. For brevity, we denote the historical simulation over 1861–1980 as “HIST”, and the historical plus RCP8.5 simulation over 1981–2100 as “RCP85” since most of this period falls under the RCP8.5 scenario. We denote the sensitivity experiment for years 1981–2100 as “RCP85_fxAMOC”, so that the difference between RCP85 and RCP85_fxAMOC shows the climate impacts of the AMOC slowdown under the chosen global warming scenario. We also test the significance of the difference between these two sets of simulations relative to internal climate variability (Zheng et al. 2019) at 95%

confidence level based on the Student's t-test between the RCP85 and RCP85_fxAMOC ensembles. This internal climate variability manifests in the inter-member difference within each ensemble. Accordingly, for each of the HIST, RCP85 and RCP85_fxAMOC simulations, we calculate the ensemble mean over five members and the ensemble spread as one standard deviation among ensemble members.

3. Results

We firstly explore the mean-state change in the tropical Pacific between the RCP85 and HIST simulations. The ensemble mean result shows an enhanced equatorial SST warming relative to the subtropics during the twenty-first century (Figure 2a). The equatorial enhanced response (Knutson & Manabe 1995; Meehl et al. 2000) to anthropogenic forcing is associated with changes in surface latent heat fluxes due to wind speed change, shortwave cloud radiation and ocean mixing (Liu et al. 2005). A warming maximum emerges at the eastern tropical Pacific and a warming minimum emerges to the south of the equator, accompanied by reduced equatorial easterlies but intensified southeast trade winds off the equator (Figure 2a), which points to the role of the wind–evaporation–SST feedback in shaping this pattern (Xie & Philander 1994; Xie et al. 2010). The interplay of different mechanisms that lead to the development of this pattern on different timescales and across different models has been discussed in Heede et al. (2020, 2021) and Heede & Fedorov (2021, 2023). The warming maximum and minimum would reach even greater amplitudes without AMOC slowdown (Figure 2b). This is because a weaker Atlantic overturning induces cooling and warming SST anomalies to the north and south of around 3^{o}S, respectively, in the eastern and central Pacific, along with anomalous cross-equatorial northerly winds (Figure 2c).

Changes in ENSO are tired to the resulting change in the mean state of the tropical Pacific (Fedorov & Philander 2000, 2001; An & Jin 2000; Jin et al. 2006; Fedorov et al. 2020). The ensemble mean of ENSO variability peaks at 4, 3.64 and 3.87 years in the HIST, RCP85 and RCP85_fxAMOC simulations, respectively, meaning that the projected anthropogenic warming shortens future ENSO period while the AMOC slowdown can make the ENSO period even shorter. On the other hand, the ensemble-mean magnitude of ENSO variability decreases over the twenty-first century under the RCP8.5 scenario, and such decrease might be even larger without the projected AMOC slowdown (Figure 1b). This result suggests that, relative to the simulated future state with reduced ENSO variability, a weakened AMOC under global warming acts to amplify ENSO variability, which is consistent with the findings of Timmermann et al. (2007a) and Dong & Sutton (2007) but is different from the study of Orihuela-Pinto et al. (2022).

Despite the ensemble-mean result showing ENSO intensification, this AMOC impact is not statistically significant relative to internal climate variability, i.e., the inter-member difference within either ensemble. Taking the 4-year period ENSO variance for example, the variance significantly (p=0.00) decreases by -47.2 ± 13.8% from the HIST to RCP85 simulation but insignificantly (p=0.39) increases by 10.6 ± 40.5% from the RCP85_fxAMOC to RCP85 simulation. The latter means that the inter-member difference within the ensembles of either simulation is greater than the ensemble-mean difference between the two global

warming simulations. In other words, ENSO variance may actually decrease between a few of the ensemble members from the RCP85_fxAMOC and RCP85 simulations, respectively.

To investigate the physical mechanisms of the AMOC on modulating future ENSO, we first examine the changes in the SST annual cycle in the eastern equatorial Pacific among the ensemble means of the HIST, RCP85 and RCP85_fxAMOC simulations. The difference between the RCP85 and HIST simulations reveals a general reduction of the SST annual cycle during the twenty-first century, though it also illustrates some anomalous semi-annual signals (Figure 2d). The difference between the RCP85_fxAMOC and HIST simulations shows a similar pattern of reduced SST annual cycle but with smaller magnitude of the reduction (Figure 2e), meaning that a weakened AMOC indeed acts to further reduce the SST annual cycle in the eastern equatorial Pacific relative to the simulated future state with an already weakened annual cycle (Figure 2f). This result is consistent with those from Timmermann et al. (2007a) and Dong & Sutton (2007), suggesting that a weakened annual cycle can lead to intensification of the ENSO amplitude and vice versa via the frequency entrainment mechanism (Chang et al. 1994; Liu 2002; Timmermann et al. 2007b). We also find that the anomalous cross-equatorial northerly winds are especially strong in May-June (Figure 2f), which indicates that a simple reduction in the mean (background) cross-equatorial winds (Hu & Fedorov 2018; Zhao & Fedorov 2020) can provide a sufficient explanation of ENSO changes in the context of an AMOC slowdown under the background of anthropogenic warming.

We further probe the physical mechanisms by which a weakened AMOC modifies ENSO by utilizing the Bjerknes (BJ) stability index (Jin et al. 2006; Manucharyan & Fedorov 2014; Zhu et al. 2017; Lu et al. 2016, 2019; Zhao & Fedorov 2020), which allows us to evaluate quantitatively the role of ocean–atmosphere feedback and damping effects. The linear equation for temperature anomalies (T_o) averaged within the mixed layer (i.e., the upper 50 m) in the tropical central and eastern equatorial Pacific (5°S–5°N, 180°E–80°W) can be written as: $\partial T_o/\partial t = BJ * T_o + \cdots$, where the omitted terms describe the term proportional to the thermocline depth in the eastern Pacific and the system's noise, and

$$BJ = -\alpha_s - \alpha_{MA} + \mu_a\beta_u\langle -\overline{T}_x\rangle + \mu_a\beta_w\langle -\overline{T}_z\rangle + \mu_a\beta_h\,\langle\frac{\overline{w}}{H_1}\rangle\,a_h \quad (1)$$

$$\text{TD} \quad \text{MA} \qquad \text{ZA} \qquad \text{EK} \qquad \text{TH}$$

From Eq. (1), the BJ index is a sum of five feedback terms: (i) the net surface heat flux feedback, or thermodynamic damping (TD), (ii) the mean advection feedback (MA), (iii) the zonal advection feedback (ZA), (iv): the Ekman upwelling feedback (EK) and (v) the thermocline feedback (TH). Terms (i) and (ii) describe negative feedback processes that damp SST anomalies. Term (iii), (v) and (iv) denote positive feedback processes that intensify SST anomalies. Together they represent the combined effects of the background state, including the mean zonal and vertical ocean temperature gradients and vertical ocean velocity ($\overline{T}_x$, $\overline{T}_z$, $\overline{w}$), atmospheric (wind stress) response to SST anomalies (μ_a), and oceanic response to equatorial wind stress anomalies (β_u, β_w and β_h) for thermocline slope, upwelling and zonal currents on the growth of ENSO SST anomalies. a_h denotes the sensitivity between

ocean subsurface temperature and sea level anomalies. H_1 denotes an effective depth for vertical advection.

We find that, consistent with the weakened ENSO variability from the HIST to RCP85 simulation, the total BJ index on average reduces by 51.6%. This reduction in the BJ index can be mostly attributed to stronger negative feedback, including the thermodynamic damping and mean advection feedback (Figure 3a,b). Moreover, if the AMOC stayed constant after the 1980s, the total BJ index would on average increase by 16.9%, which is consistent with the strengthening of ENSO variability from the RCP85_fxAMOC to RCP85 simulation. This relative increase in the BJ index is mainly caused by stronger positive Ekman upwelling feedback (Figure 3a,b), which results from enhanced atmospheric wind stress response to SST anomalies (μ_a) and enhanced oceanic upwelling response to equatorial wind stress anomalies (β_w) (Figure 3c). Note that while β_h and μ_a have comparable percentage increases, the contribution from the thermocline feedback is small compared to that from the Ekman upwelling feedback.

Next, we investigate the impacts of AMOC slowdown on ENSO diversity, focusing on events characterized by the Eastern Pacific (EP) or Central Pacific (CP) patterns with maximum SST anomalies developing in the eastern and central Pacific, respectively (Yu & Kao 2007; Ashok et al. 2007; Kao & Yu 2009; Takahashi et al. 2011; Capotondi et al. 2015; Santoso et al. 2019). To determine the type of particular El Niño events, we follow Takahashi et al. (2011) and firstly compute empirical orthogonal functions (EOFs) for the detrended monthly SST anomalies (relative to the SST climatology of the base period for each observation or model simulation) for the observations and for the HIST, RCP85 and RCP85_fxAMOC simulations over a domain bounded by 10°S–10°N and the Pacific lateral boundaries. We focus on the first two principal components (PC1 and PC2), which are normalized by the standard deviation for the base period and smoothed with a 1-2-1 filter. The dimensional spatial SST patterns of EOF1 and EOF2 are then obtained by linearly regressing SST anomalies onto PC1 and PC2 (Figure S2).

Next, following Takahashi et al. (2011), we calculate the E and C indices for ENSO as

$$E = \frac{PC1-PC2}{\sqrt{2}} \quad (2)$$

$$C = \frac{PC1+PC2}{\sqrt{2}} \quad (3)$$

These two indices describe the strength of EP and CP El Niño events, respectively. We linearly regress SST anomalies onto the E and C indices to obtain the dimensional spatial SST patterns corresponding to EP and CP El Niño events (Figure 4). The ensemble mean of observations for years 1861–1980 displays an EP pattern with maximum SST anomalies in the eastern equatorial Pacific and along the coast of Peru (Figure 4a) and a CP pattern with maximum SST anomalies over the central equatorial Pacific (Figure 4b). CCSM4 captures the general features of both EP and CP patterns seen in the observations during this period except with slightly large amplitudes of the EP pattern (Figure 4c) and a more westward maximum in the CP pattern (Figure 4d), which is similar to other climate model simulations

(Yu & Kim 2010; Kim & Yu 2012). During the twenty-first century, the SST anomaly maximum is projected to weaken for the EP pattern (Figure 4e) and to move westward for the CP pattern (Figure 4f) under the RCP8.5 scenario. Without the AMOC slowdown, the SST anomaly maximum would reduce even more for EP events (Figure 4g) and shift even more westward for CP events (Figure 4h).

We further employ the EP and CP indices to assess the frequency of El Niño events of different types. We define an EP or CP warm event when the corresponding averaged October–March index exceeds one standard deviation (Orihuela-Pinto et al. 2022). Observations show more CP than EP events (about three fifths versus two fifths of the total number of warm events) between 1861 and 1980; the HIST simulation exhibits generally similar percentages of CP and EP events (Figure 4i). Since the 1980s, the RCP85 simulation suggests that CP El Niño events are more frequent than the EP events. If the AMOC did not weaken, the proportion of CP to EP ENSO events would on average further increase by 11.0% over 1981–2100 (Figure 4i), which is consistent with the result from Orihuela-Pinto et al. (2022). However, this AMOC impact of shifting El Niño events toward the CP type is statistically insignificant ($p=0.29$) relative to internal climate variability.

4. Conclusion and discussions

In this study, we isolate and quantify the AMOC impacts on ENSO in a warming climate using CCSM4 simulations. We find that the weakened AMOC causes a reduction in the SST annual cycle in the eastern equatorial Pacific and anomalous cross-equatorial northerly winds there, which leads to an increase in ENSO variance by around 11% between 1981 and 2100 relative to the simulated ENSO weakening induced by anthropogenic warming. We further analyze the Bjerknes stability index and find that this ENSO intensification induced by the AMOC slowdown can be primarily attributed to the enhanced Ekman upwelling feedback related to amplified atmospheric response to SST anomalies as well as oceanic upwelling response to equatorial wind stress anomalies. We also find that the weakened AMOC modulates ENSO complexity by increasing the ratio of CP to EP events by approximately 11%. Nevertheless, both AMOC effects on ENSO magnitude and type are relatively small when compared to ENSO variations driven by internal climate variability.

It is noteworthy that the AMOC impacts on ENSO presented in our study are considered in the context of anthropogenic warming over the twenty-first century during which the AMOC will slow down but remain active, which are thus different from the impacts of a collapsed AMOC that is often considered in the paleoclimate context using idealized strong freshwater hosing experiments (Timmermann et al. 2007a; Dong & Sutton 2007; Orihuela-Pinto et al. 2022). It also merits attention that, compared to the AMOC modest impact on ENSO induced SST variance (Figure S3g), the weakened overturning has a greater impact on interannual SST skewness and hence ENSO asymmetry (Figure S3h). Over 1981–2100, the weakened AMOC generally reduces the ENSO skewness by decreasing positive SST skewness in the eastern Pacific and at the same time increasing negative skewness in the western Pacific. The maximum change in skewness can exceed 30% of its historical values (Figure S3b, h).

We note that the simulated AMOC-induced changes in ENSO variability and the role of ocean–atmosphere feedback are opposite in our study and that of Orihuela-Pinto et al. (2022), which may reflect the delicate balance of amplifying and damping feedback in different model simulations. We also find significant differences in the AMOC-induced mean state changes in zonal winds and thermocline along the equatorial Pacific (Figure S4) between our study and Orihuela-Pinto et al. (2022), which to some extent reflects the model uncertainty as reported in Timmermann et al. (2007a). Additionally, a recent study by Lee et al. (2021) has suggested that large (≥50) ensembles are needed to robustly capture the baseline ENSO characteristics and physical processes. Given the large uncertainties in the IPCC AR5 model projections of ENSO intensity and the need of large ensembles, it would be important to apply the current framework to the state-of-art IPCC AR6 model large ensemble simulations to further tackle this scientific question.

Acknowledgments

This work is supported by grants to W.L. from U.S. National Science Foundation (AGS-2053121, OCE-2123422 and AGS-2237743). W.L. is also supported by the Hellman Fellows Fund as a Hellman Fellow. AVF is supported by NSF (AGS-2053096), NOAA (NA20OAR4310377), DOE (DE-SC0023134), and by the ARCHANGE project of the "Make our planet great again" program (ANR-18-MPGA-0001, France). The CESM/ CCSM4 project has been supported primarily by the National Science Foundation (NSF). This material is based upon work supported by the National Center for Atmospheric Research, which is a major facility sponsored by the NSF under Cooperative Agreement No. 1852977.

Open Research

Data Availability Statement

COBE-SST2 data are publically available at https://ds.data.jma.go.jp/tcc/tcc/products/elnino/cobesst/cobe-sst.html

ERSSTv4 & v5 data are publically available at https://www.ncei.noaa.gov/products/extended-reconstructed-sst

KAPLAN EXTENDED v2 data are publically available at https://iridl.ldeo.columbia.edu/SOURCES/.KAPLAN/.EXTENDED/.v2/.ssta/datafiles.html?Set-Language=en

The source code of CCSM4 is available at https://www.cesm.ucar.edu/models/ccsm4.0/

Model configuration parameters used to run the model experiment are available in Liu et al. (2020), https://www.science.org/doi/10.1126/sciadv.aaz4876

The data to generate Figures 1-4 are available at Zenodo DOI: https://doi.org/10.5281/zenodo.7783335

References

1. An, S.-I. & Jin, F.F. (2000), An eigen analysis of the interdecadal changes in the structure and frequency of ENSO mode. Geophys. Res. Lett., 27, 2573–2576.
2. Ashok, K., Behera, S.K., Rao, S.A., Weng, H. & Yamagata, T. (2007), El Niño Modoki and its possible teleconnection. J. Geophys. Res., 112, C11007.
3. Bryden, H. & Imawaki, S. (2001), Ocean heat transport. Ocean Circulation and Climate, G. Siedler, J. Church, and J. Gould, Eds., International Geophysics Series, Vol. 77, Academic Press, 317–336.
4. Caesar, L., Rahmstorf, S., Robinson, A., Feulner, G. & Saba, W. (2018), Observed fingerprint of a weakening Atlantic Ocean overturning circulation. Nature, 556, 191–196.
5. Caesar, L., McCarthy, G.D., Thornalley, D.J.R., Cahill, N. & Rahmstorf, S. (2021), Current Atlantic Meridional Overturning Circulation weakest in last millennium. Nat. Geosci., 14, 118–120.
6. Cai, W. et al. (2015), ENSO and greenhouse warming. Nat. Clim. Chang., 5, 849–859.
7. Cai, W., Ng, B., Wang, G., Santoso, A., Wu, L. & Yang, K. (2022), Increased ENSO sea surface temperature variability under four IPCC emission scenarios. Nat. Clim. Chang., 12, 228–231.
8. Capotondi, A. (2013), ENSO diversity in the NCAR CCSM4 climate model. J. Geophys. Res. Oceans, 118, 4755–4770.
9. Chang, P., Wang, B., Li, T. & Ji, L. (1994), Interactions between the seasonal cycle and the southern oscillation—Frequency entrainment and chaos in a coupled ocean-atmosphere model. Geophys. Res. Lett., 21, 2817–2820.
10. Collins, M. et al. (2010), The impact of global warming on the tropical Pacific Ocean and El Niño. Nat. Geosci., 3, 391–397.
11. Delworth, T.L. & Dixon, K.W. (2006), Have anthropogenic aerosols delayed a greenhouse gas-induced weakening of the North Atlantic thermohaline circulation? Geophys. Res. Lett., 33, L02606.
12. Deser, C. et al. (2012), ENSO and Pacific decadal variability in the Community Climate System Model version 4. J. Clim., 25, 2622–2651.
13. Dong, B.-W. & Sutton, R.T. (2002), Adjustment of the coupled ocean–atmosphere system to a sudden change in the Thermohaline Circulation. Geophys. Res. Lett., 29, L1728.
14. Dong, B.-W. & Sutton, R.T. (2007), Enhancement of ENSO variability by a weakened Atlantic thermohaline circulation in a coupled GCM. J. Clim., 20, 4920–4939.
15. Fedorov, A.V. & Philander, S.G. (2000), Is El Niño changing?. Science, 288, 1997–2002.
16. Fedorov, A.V. & Philander, S.G. (2001), A stability analysis of tropical ocean–atmosphere interactions: Bridging measurements and theory for El Niño. J. Clim., 14, 3086–3101.
17. Fedorov, A.V., Hu, S., Wittenberg, A.T., Levine, A.F. & Deser, C. (2020), ENSO Low-Frequency Modulation and Mean State Interactions. El Niño Southern Oscillation in a changing climate, pp.173–198.

18. Frajka-Williams, E. (2015), Estimating the Atlantic overturning at 26°N using satellite altimetry and cable measurements. Geophys. Res. Lett., 42, 3458–3464.
19. Hassan, T., Allen, R.J., Liu, W. & Randles, C.A. (2021), Anthropogenic aerosol forcing of the Atlantic meridional overturning circulation and the associated mechanisms in CMIP6 models. Atmos. Chem. Phys., 21, 5821–5846.
20. Heede, U.K., Fedorov, A.V. & Burls, N.J. (2020), Time scales and mechanisms for the tropical Pacific response to global warming: A tug of war between the ocean thermostat and weaker walker. J. Clim., 33, 6101–6118.
21. Heede, U.K. & Fedorov, A.V. (2021), Eastern equatorial Pacific warming delayed by aerosols and thermostat response to CO_2 increase. Nat. Clim. Chang., 11, 696–703.
22. Heede, U.K., Fedorov, A.V. & Burls, N.J. (2021), A stronger versus weaker Walker: understanding model differences in fast and slow tropical Pacific responses to global warming. Clim. Dyn., 57, 2505–2522.
23. Heede, U.K. & Fedorov, A.V. (2023), Colder eastern equatorial Pacific and stronger Walker circulation in the early 21st century: Separating the forced response to global warming from natural variability. Geophys. Res. Lett., 50, e2022GL101020.
24. Hirahara, S., Ishii, M. & Fukuda, Y. (2014), Centennial-scale sea surface temperature analysis and its uncertainty. J. Clim., 27, 57–75.
25. Hu, S. & Fedorov, A.V. (2018), Cross-equatorial winds control El Niño diversity and change. Nat. Clim. Chang., 8, 798.
26. Huang, B. et al. (2015), Extended Reconstructed Sea Surface Temperature version 4 (ERSST.v4). Part I: Upgrades and Intercomparsions. J. Clim., 28, 911–930.
27. Huang, B. et al. (2017), Extended reconstructed sea surface temperature, version 5 (ERSSTv5): upgrades, validations, and intercomparisons. J. Clim., 30, 8179–8205.
28. IPCC, 2013: Climate Change 2013: The Physical Science Basis. Contribution of Working Group I to the Fifth Assessment Report of the Intergovern- mental Panel on Climate Change [Stocker, T.F., D. Qin, G.-K. Plattner, M. Tignor, S.K. Allen, J. Boschung, A. Nauels, Y. Xia, V. Bex and P.M. Midgley (eds.)]. Cambridge University Press, Cambridge, United Kingdom and New York, NY, USA, 1535 pp.
29. IPCC, 2021: Climate Change 2021: The Physical Science Basis. Contribution of Working Group I to the Sixth Assessment Report of the Intergovernmental Panel on Climate Change [Masson-Delmotte, V., P. Zhai, A. Pirani, S.L. Connors, C. Péan, S. Berger, N. Caud, Y. Chen, L. Goldfarb, M.I. Gomis, M. Huang, K. Leitzell, E. Lonnoy, J.B.R. Matthews, T.K. Maycock, T. Waterfield, O. Yelekçi, R. Yu, and B. Zhou (eds.)]. Cambridge University Press, Cambridge, United Kingdom and New York, NY, USA, 2391 pp.
30. Jin, F.-F., Kim, S.T. & Bejarano, L. (2006), A coupled-stability index for ENSO. Geophys. Res. Lett., 33, L23708.
31. Kaplan, A. et al. (1998), Analyses of global sea surface temperature 1856-1991, J. Geophys. Res. Oceans, 103, 18567–18589.
32. Kao, H.-Y. & Yu, J.-Y. (2009), Contrasting eastern-Pacific and central-Pacific types of ENSO. J. Clim., 22, 615–632.

33. Kilbourne, K.H. et al. (2022), Atlantic circulation change still uncertain. Nat. Geosci., 15, 165–167.
34. Kim, S.T. & Yu, J.-Y. (2012), The two types of ENSO in CMIP5 models. Geophys. Res. Lett., 39, L11704
35. Knutson, T.R. & Manabe S. (1995), Time-mean response over the tropical Pacific to increased CO_2 in a coupled ocean–atmosphere model. J. Clim., 8 , 2181–2199.
36. Lee, J. et al. (2021), Robust evaluation of ENSO in climate models: How many ensemble members are needed? Geophys. Res. Lett., 48, e2021GL095041.
37. Li, S. & Liu, W. (2022), Impacts of Arctic sea ice loss on global ocean circulations and interbasin ocean heat exchanges. Clim. Dyn., 59, 2701–2716.
38. Liu, W. et al. (2015), Extended Reconstructed Sea Surface Temperature version 4 (ERSST.v4). Part II: Parametric and Structural Uncertainty Estimations. J. Clim., 28, 931–951.
39. Liu, W., Xie, S.-P., Liu, Z. & Zhu, J. (2017), Overlooked possibility of a collapsed Atlantic Meridional Overturning Circulation in warming climate. Sci. Adv., 3, e1601666.
40. Liu, W., Fedorov, A.V., Xie, S.-P. & Hu, S. (2020), Climate impacts of a weakened Atlantic Meridional Overturning Circulation in a warming climate. Sci. Adv., 6, eaaz4876.
41. Liu, Z. (2002), A simple model study of the forced response of ENSO to an external periodic forcing. J. Clim., 15, 1088–1098.
42. Liu, Z., Vavrus, S., He, F., Wen, N. & Zhong, Y. (2005), Rethinking tropical ocean response to global warming: The enhanced equatorial warming. J. Clim., 18, 4684–4700.
43. Lu, Z., Liu, Z. & Zhu, J. (2016), Abrupt intensification of ENSO forced by deglacial ice-sheet retreat in CCSM3. Clim. Dyn., 46, 1877–1891.
44. Lu, Z., Liu, Z., Chen, G. & Guan, J. (2019), Prominent precession band variance in ENSO intensity over the last 300,000 years. Geophys. Res. Lett., 46, 9786–9795.
45. Manucharyan, G.E. & Fedorov, A.V. (2014), Robust ENSO across a wide range of climates. J. Clim., 27, 5836–5850.
46. Meehl, G.A. et al. (2000), Response of the NCAR Climate System Model to increased CO_2 and the role of physical processes. J. Clim., 13, 1879–1898.
47. Menary, M.B. et al. (2020), Aerosol-forced AMOC changes in CMIP6 historical simulations. Geophys. Res. Lett., 47, e2020GL088166.
48. Orihuela-Pinto, B., Santoso, A., England, M.H. & Taschetto, A.S. (2022), Reduced ENSO Variability due to a Collapsed Atlantic Meridional Overturning Circulation. J. Clim., 35, 5307–5320.
49. Rahmstorf, S. et al. (2015), Exceptional twentieth-century slowdown in Atlantic Ocean overturning circulation. Nat. Clim. Chang., 5, 475–480.
50. Ren, X. & Liu, W. (2021), The role of a weakened Atlantic meridional overturning circulation in modulating marine heatwaves in a warming climate. Geophys. Res. Lett., 48, e2021GL095941.

51. Roberts, C.D., Jackson, L. & McNeall, D. (2014), Is the 2004–2012 reduction of the Atlantic meridional overturning circulation significant? Geophys. Res. Lett., 41, 3204–3210.
52. Santoso, A. et al. (2019), Dynamics and predictability of El Niño–Southern Oscillation: An Australian perspective on progress and challenges. Bull. Amer. Meteor. Soc., 100, 403–420.
53. Smeed, D.A. et al. (2018), The North Atlantic Ocean is in a state of reduced overturning. Geophys. Res. Lett., 45, 1527–1533.
54. Stevenson, S.L. (2012), Significant changes to ENSO strength and impacts in the twenty-first century: Results from CMIP5. Geophys. Res. Lett., 39, L17703.
55. Takahashi, K., Montecinos, A., Gou-banova, K. & Dewitte, B. (2011), ENSO regimes: Reinterpreting the canonical and Modoki El Niño, Geophys. Res. Lett., 38, L10704.
56. Thornalley, D.J.R. et al. (2018), Anomalously weak Labrador Sea convection and Atlantic overturning during the past 150 years. Nature, 556, 227–230.
57. Timmermann, A. et al. (2007a), The influence of a weakening of the Atlantic meridional overturning circulation on ENSO. J. Clim., 20, 4899–4919.
58. Timmermann, A., Lorenz, S., An, S.-I., Clement, A. & Xie, S.-P. (2007b), The effect of orbital forcing on the mean climate and variability of the tropical Pacific. J. Clim., 20, 4147–4159.
59. Xie, S-P. & Philander, S.G.H. (1994), A coupled ocean-atmosphere model of relevance to the ITCZ in the eastern Pacific. Tellus, 46A , 340–350.
60. Xie, S.-P. et al. (2010), Global warming pattern formation: Sea surface temperature and rainfall. J. Clim., 23, 966–986.
61. Weijer, W., Cheng, W., Garuba, O.A., Hu, A. & Nadiga, B.T. (2020), CMIP6 models predict significant 21st century decline of the Atlantic Meridional Overturning Circulation. Geophys. Res. Lett., 47, e2019GL086075.
62. Williamson, M.S. et al. (2018), Effect of AMOC collapse on ENSO in a high resolution general circulation model. Clim. Dyn., 50, 2537–2552.
63. Yu, J.-Y. & Kao, H.-Y. (2007), Decadal changes of ENSO persistence barrier in SST and ocean heat content indices: 1958–2001. J. Geophy. Res.: Atmos., 112, D13106.
64. Yu, J.-Y. & Kim, S.T. (2010), Identification of Central-Pacific and Eastern-Pacific types of ENSO in CMIP3 models. Geophys. Res. Lett., 37, L15705.
65. Zhang, R. & Delworth, T. (2005), Simulated tropical response to a substantial weakening of the Atlantic thermohaline circulation. J. Clim., 18, 1853–1860.
66. Zhao, B. & Fedorov, A.V. (2020), The Effects of Background Zonal and Meridional Winds on ENSO in a Coupled GCM. J. Clim., 33, 2075–2091.
67. Zheng, X.-T., Xie, S.-P., Lv, L.-H. & Zhou, Z.-Q. (2016), Intermodel uncertainty in ENSO amplitude change tied to Pacific Ocean warming pattern. J. Clim., 29, 7265–7279.
68. Zheng, X.-T., Hui, C. & Yeh, S.W. (2019), Response of ENSO amplitude to global warming in CESM large ensemble: uncertainty due to internal variability. Clim. Dyn., 50, 4019–4035.

533 69. Zhu, J. et al. (2017), Reduced ENSO variability at the LGM revealed by an isotope-
534 enabled Earth system model. Geophys. Res. Lett., 44, 6984–6992.

Figures

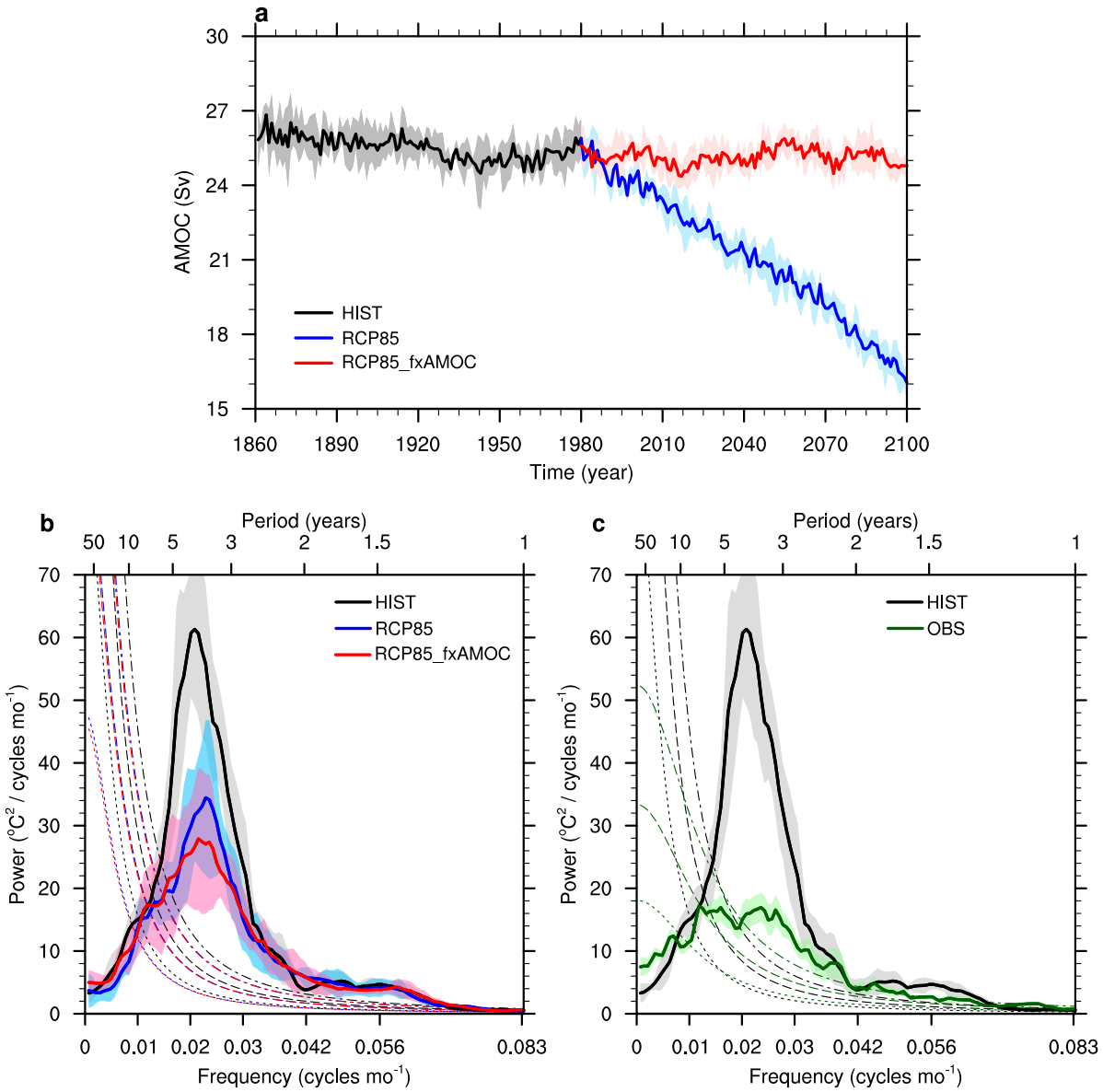

Figure 1. (a) AMOC strength in the HIST simulation for years 1861–1980 (black), RCP85 simulation for 1981–2100 (blue), and RCP85_fxAMOC simulation for 1981–2100 (red). AMOC strength is defined as the maximum of the annual mean stream function below 500 m in the North Atlantic. (b) Power spectra of the Niño 3.4 indices in the HIST (black), RCP85 (blue) and RCP85_fxAMOC (red) simulations and associated 95% confidence limits (dashed/dotted curves). (c) Power spectra of the Niño 3.4 indices in the HIST (black) and observations (green) over 1861–1980. In all cases solid lines denote ensemble-mean results, and light color shading indicates ensemble spread.

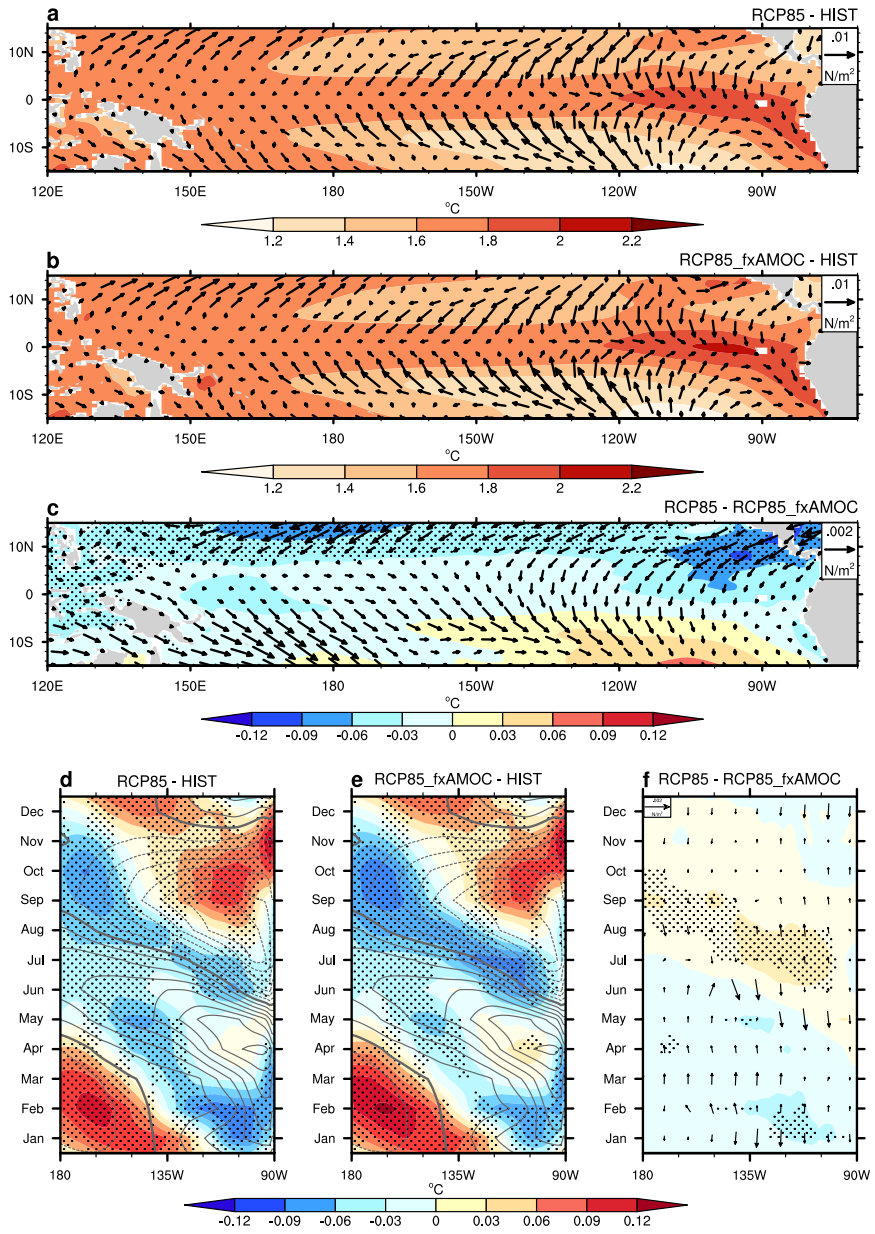

Figure 2. (a-c) Ensemble-mean differences of annual mean SST (color shading, in ^{o}C) and surface wind stress (vectors, in N/m^2) between (a) the RCP85 and HIST simulations, (b) RCP85_fxAMOC and HIST simulations, and (c) RCP85 and RCP85_fxAMOC simulations. (d-f) Hovmöller diagrams showing ensemble-mean differences for the annual cycle of SST (color shading, in ^{o}C) in the tropical Pacific (5^{o}S-5^{o}N) between (d) RCP85 and HIST simulations, (e) RCP85_fxAMOC and HIST simulations, and (f) RCP85 and RCP85_fxAMOC simulations. The annual cycle of SST from the HIST simulation (contours in ^{o}C with a contour interval of 0.2^{o}C; positive solid, negative dashed and zero contours thickened) is overlaid in panels (d) and (e). The ensemble-mean difference for the annual cycle of surface wind stress (vectors, in N/m^2) between RCP85 and RCP85_fxAMOC simulations is superposed in panel (f). Note the anomalous northerly winds during May-June in panel (f). Stippling in panels (c)-(f) indicate where SST differences are statistically significant at a 95% confidence level based on Student's t-test.

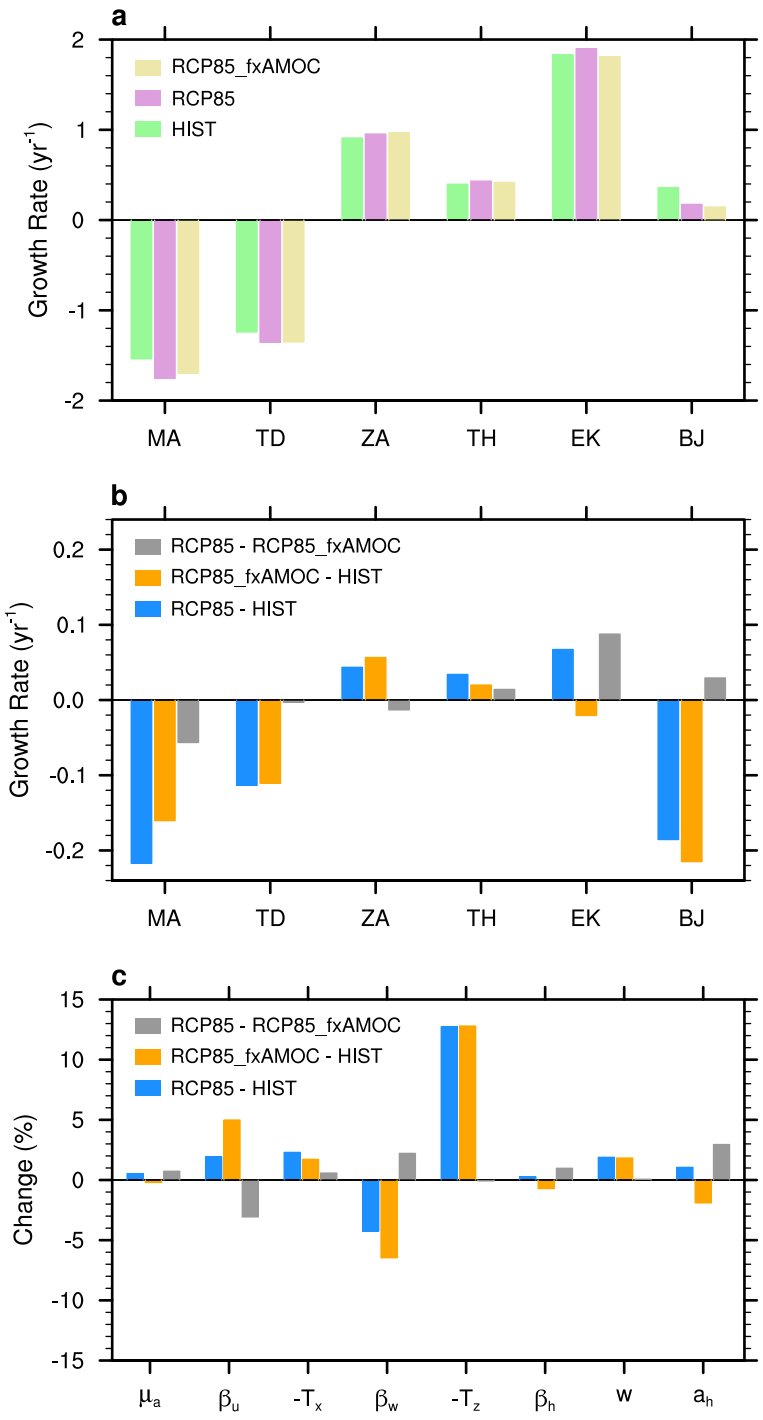

Figure 3. (a) The BJ index for the HIST (green), RCP85 (purple) and RCP85_fxAMOC (yellow) simulations. MA, TD, ZA, TH, and EK represent the mean advection, thermal damping, zonal advection, thermocline, and Ekman feedback, respectively. The panel shows the ensemble-mean result. (b) Similar to panel (a) but for changes between simulations (RCP85 – HIST, blue; RCP85_fxAMOC – HIST, orange; RCP85 – RCP85_fxAMOC, gray). (c) Similar to panel (b) but for changes in percentage of different regression coefficients and mean temperature gradients relative to HIST.

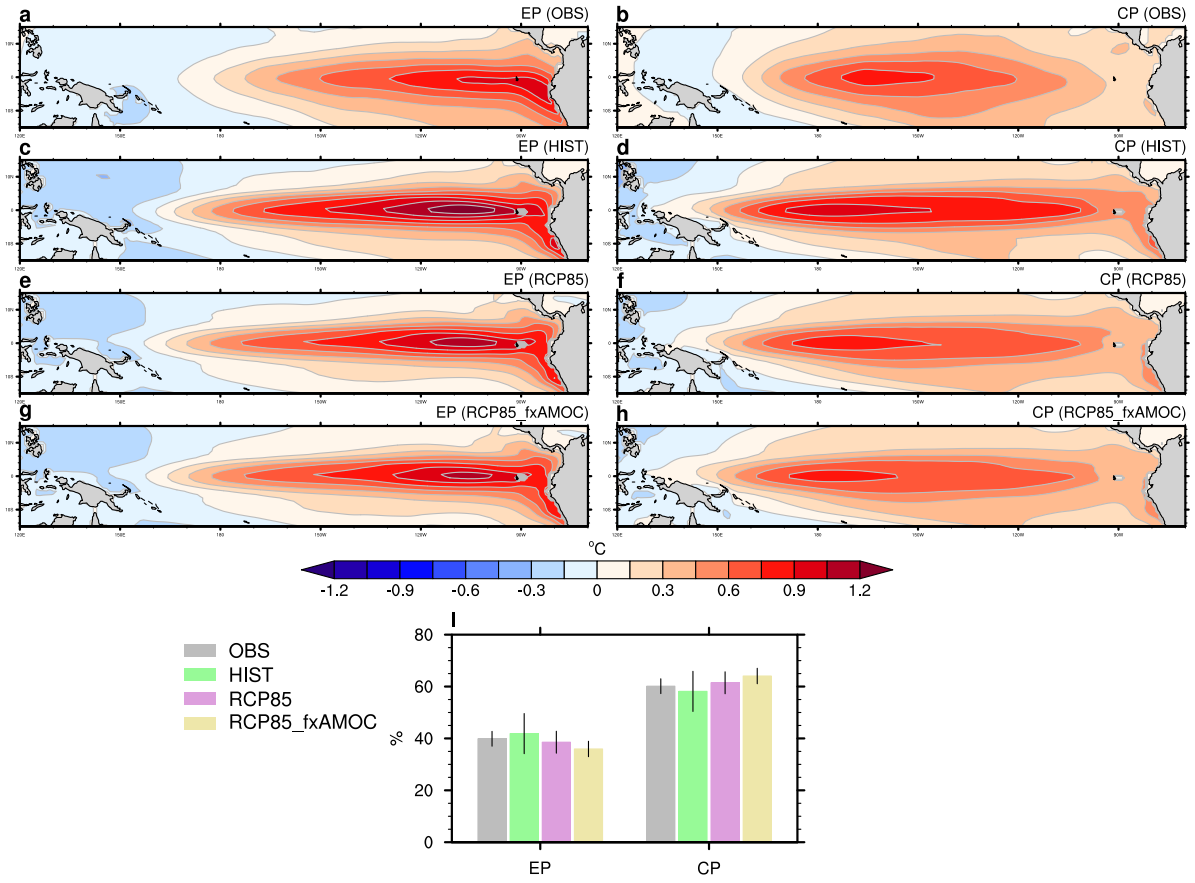

Figure 4. (a,c,e,g) Linear regression of SST anomalies (color shading, in °C) onto the E-index for (a) observations, (c) the HIST simulation for years 1861–1980, and (e) RCP85 and (g) RCP85_fxAMOC simulations, both for years 1981–2100. The panels show ensemble-mean results. (b,d,f,h) As in the left panels but for the SST regression onto the C-index. (i) The fraction of EP and CP El Niño events in the observations (gray), in the HIST simulation (green) for 1861–1980, and in the RCP85 (purple) and RCP85_fxAMOC (yellow) simulations for 1981–2100. Bars denote one standard deviation.